

See discussions, stats, and author profiles for this publication at: <https://www.researchgate.net/publication/223968048>

# Nanotoxicity of Gold and Gold-Cobalt Nanoalloy

ARTICLE *in* CHEMICAL RESEARCH IN TOXICOLOGY · APRIL 2012

Impact Factor: 3.53 · DOI: 10.1021/tx300053h · Source: PubMed

---

CITATIONS

16

---

READS

68

## 5 AUTHORS, INCLUDING:



Emad Girgis

Harvard University

51 PUBLICATIONS 637 CITATIONS

[SEE PROFILE](#)



Wagdy K B Khalil

National Research Center, Egypt

75 PUBLICATIONS 267 CITATIONS

[SEE PROFILE](#)



Mona B. Mohamed

Cairo University

76 PUBLICATIONS 3,680 CITATIONS

[SEE PROFILE](#)



K V Rao

KTH Royal Institute of Technology

468 PUBLICATIONS 6,361 CITATIONS

[SEE PROFILE](#)

## Nanotoxicity of Gold and Gold–Cobalt Nanoalloy

E. Grgis,\*†‡ W. K. B. Khalil,§ A. N. Emam,‡|| M. B. Mohamed,⊥ and K. V. Rao#

† Solid State Physics Department, National Research Center, 12622 Dokki, Giza, Egypt

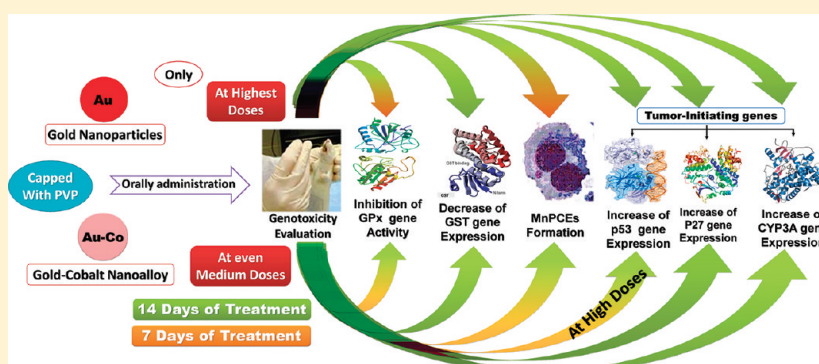
‡ Advanced Materials and Nanotechnology Lab, CEAS, National Research Center, 12622 Dokki, Giza, Egypt

§ Cell Biology Department, National Research Center, 12622 Dokki, Giza, Egypt

|| Biomaterials Department, National Research Center, 12622 Dokki, Giza, Egypt

⊥ National Institute of Laser Enhanced Science, Cairo University, Egypt

# Department of Materials Science, Royal Institute of Technology, Stockholm SE-100 44, Sweden



**ABSTRACT:** Nanotoxicology test of gold nanoparticles (Au NPs) and gold–cobalt (Au–Co) nanoalloy is an important step in their safety evaluation for biomedical applications. The Au and Au–Co NPs were prepared by reducing the metal ions using sodium borohydride ( $\text{NaBH}_4$ ) in the presence of polyvinyl pyrrolidone (PVP) as a capping material. The average size and shape of the nanoparticles (NPs) were characterized using high resolution transmission electron microscopy (HRTEM). Cobalt presence in the nanoalloy was confirmed by energy dispersive X-ray spectroscopy (EDX) analysis, and the magnetic properties of these particles were determined using a vibrating sample magnetometer (VSM). The Gold and gold–cobalt NPs of average size  $15 \pm 1.5$  nm were administered orally to mice with a dose of 80, 160, and 320 mg/kg per body weight (bw) using gavages. Samples were collected after 7 and 14 days of the treatment. The results indicated that the Au–Co NPs were able to induce significant alteration in the tumor-initiating genes associated with an increase of micronuclei (MNs) formation and generation of DNA adduct (8-hydroxy-2-deoxyguanosine, 8-OHdG) as well as a reduction in the glutathione peroxidase activity. This action of Au–Co NPs was observed using 160 and 320 mg/kg bw at both time intervals. However, Au NPs had much lower effects than Au–Co NPs on alteration in the tumor-initiating genes, frequency of MNs, and generation of 8-OHdG as well as glutathione peroxidase activity except with the highest dose of Au NPs. This study suggests that the potential to cause in vivo genetic and antioxidant enzyme alterations due to the treatment by Au–Co nanoalloy may be attributed to the increase in oxidative stress in mice.

### 1. INTRODUCTION

The range of different types and the total number of manufactured nanomaterials used for technical applications and in consumer products are quickly increasing and represent a potential source of emerging contaminants in the environment. Nanoparticles are defined as having two or three dimensions in the size range of 1–100 nm<sup>1</sup> that exhibit special physical and chemical properties compared to their bulk materials.<sup>2</sup> Such properties include elevated reactivity due to a large surface to volume ratio with a more reactive surface,<sup>3</sup> which raises concerns about the toxicity of nanomaterials to humans and wildlife.<sup>4</sup>

Gold nanoparticles (Au NPs), which are readily taken up by cells,<sup>5</sup> have one of their major applications in the medical

sector, where they are proposed as new tools in diagnostic investigations,<sup>6</sup> and drug delivery systems.<sup>7</sup> Different findings regarding the cytotoxicity of Au NPs have been published depending on the size and coating of particles used and the measured end points. Particle size dependent toxicity of Au NPs toward different cell types has been reported by Pan et al.; they noticed that smaller particles are more toxic than larger ones.<sup>8</sup> In contrast to this finding, Connor et al.<sup>9</sup> could not detect cytotoxic effects in a human leukemia cell line exposed to Au NPs. Negative effects to cytoskeletal components yet a reduction in cell growth in human dermal fibroblasts have also

Received: February 6, 2012

Published: April 9, 2012

been reported<sup>10</sup> along with enhanced reactive oxygen species (ROS) levels in exposed bivalves.<sup>11</sup>

Investigating the effect of cobalt nanoparticles (Co NPs) on genetic alteration was done in several studies. For example, it has been reported that Co NPs were capable of inducing genetic damage in human peripheral blood leukocytes at a dose of 40 mM.<sup>12</sup> Given that the fate of Co NP once internalized in cells is unknown, there is the possibility that they may corrode over time, releasing cobalt ions (Co<sup>2+</sup> ions); hence, it is important to consider the biological effect of these ions. Indeed, it has been demonstrated that Co<sup>2+</sup> ions can produce clastogenic responses typified by single strand breaks, chromosomal aberrations, sister-chromatid exchanges, and covalent DNA–protein cross-links through mechanisms involving oxidative stress and the inhibition of DNA repair.<sup>13,14</sup> These studies are vital, as cobalt exposure alone or in combination with other metal particles has been shown to be associated with various lung diseases (interstitial pneumonitis, fibrosis, asthma, and lung cancer) that progress at a slow rate and take time to manifest.<sup>15,16</sup> Furthermore, in a study evaluating the pro-inflammatory effect of different nanoparticles on endothelial cells, higher IL-8 expression was induced by Co NP as compared to silicon dioxide and titanium dioxide, and was thought to be due to the release of Co<sup>2+</sup> ions from the Co NP, which are known to be potent inducers of IL-8.<sup>17</sup> Hence, the long-term consequence of metallic nanoparticle uptake is certainly an issue that needs to be addressed.

Designing nanomaterials for biomedical applications such as cancer therapy and imaging, drug delivery, and smart targeting is one of our main concerns. It is crucial to study the genotoxic effect of these particles and determine the safe dose. Therefore, the aim of this study is to evaluate the genotoxic effect of Au and Au–Co NPs. However, the potential dose-induced toxicity of such NPs on the mammalian cells *in vivo* should be first evaluated. Therefore, the main objective of this study is to determine if pure Au and Au–Co NPs could (a) alter the expression of tumor-initiating genes, (b) induce MNs formation, (c) induce genomic damage caused by oxidative stress (8-OHdG), and (d) inhibit the activity of antioxidant enzymes in male mice. To investigate the influence of these nanoparticle characteristics on toxicity, the morphology (size and shape) of the used particles within different media was determined prior to performing the toxicity studies.

## 2. EXPERIMENTAL PROCEDURES

**2.1. Materials.** The materials used in this study were hydrogen tetrachloroaurate (III) trihydrate (HAuCl<sub>4</sub>·3H<sub>2</sub>O, Aldrich, 99.999%), cobalt acetate (Co(CH<sub>3</sub>COO)<sub>2</sub>, WINLAB, 98%), polyvinyl pyrrolidone (PVP, ICN Biomedicals, Inc., Av. Wt 30,000–40,000), sodium borohydride (NaBH<sub>4</sub>, WINLAB, 98%), and purified water from the Millipore Milli-Q water purification system.

Gold nanoparticles (Au NPs) were prepared by a chemical reduction of HAuCl<sub>4</sub>·3H<sub>2</sub>O using NaBH<sub>4</sub> as a reducing agent as reported previously, with little modification.<sup>18–21</sup> An aqueous solution of HAuCl<sub>4</sub>·3H<sub>2</sub>O (1 mM, 10 mL) with 1.0 g of PVP was brought to reflux during stirring, and then 2 mL of 1 mM ice cooled NaBH<sub>4</sub> solution was added dropwise under vigorous stirring to prevent inhomogeneous growth and aggregation. The color of the solution changed from pale yellow to deep red indicating the formation of the Au NPs. The solution was left for an additional 15 min at room temperature to obtain uniform mixing and good size distribution.

Gold–cobalt alloyed nanoparticles (Au–Co NPs) have been prepared in the same way but by substituting predetermined moles of cobalt atoms in the form of cobalt acetate (i.e., mixed particles are with cobalt mole fractions  $x_{\text{Co}}$  of 0.5), using chemical reduction for

both of Au<sup>3+</sup> and Co<sup>2+</sup> ions precursors within the same time, using a reducing agent (i.e., NaBH<sub>4</sub>).<sup>22</sup> In this typical method, 10 mL of NaBH<sub>4</sub> aqueous solution (1 mM) was added dropwise into a solution containing a mixture of HAuCl<sub>4</sub>·3H<sub>2</sub>O (1 mM, 5 mL) and Co(CH<sub>3</sub>COO)<sub>2</sub> (1 mM, 5 mL) with 1.0 g of PVP, which act as capping materials under vigorous stirring at 70 °C. The color of the solution changed from faint pink to deep red, indicating the formation of the Au–Co NPs. The mixture was kept under stirring and refluxing at 70 °C for 10 min and then cooled down to room temperature. Different sizes of Au–Co NPs have been obtained in the same way as that mentioned previously, but by changing the molar ratio of reducing agent  $R$  of 1.0, 0.5, and 0.25 (i.e.,  $R = \text{BH}_4^-/\text{Au}^{3+}$ , Co<sup>2+</sup> ion precursors) as mentioned previously to obtain different sizes of Co, Au, or Au–Co bimetallic NPs.<sup>22–24</sup>

The morphology and high resolution lattice images of the samples have been investigated using HRTEM JEOL-JEM-2100 LB<sub>6</sub>. The EDX analysis for the detection of characteristic X-rays for elemental analysis is determined using an X-Max 80 detector unit which was equipped with transmission electron microscope (TEM) JEM-1230. The UV-visible absorption spectra of the prepared samples have been investigated using an Ocean Optics USB 650 Fiber optics spectrometer. In addition, the concentration of Au and Au–Co NPs were determined spectroscopically according to Haiss et al.<sup>25</sup> The magnetic measurements were carried out using a vibrating sample magnetometer (VSM) (ADE Technologies, Inc., EV11 (model 8810)). Particle size and distribution of the original solution and the concentrated solution were measured by dynamic light scattering (DLS), using Malvern Zetasizer Nano-ZS (Malvern Instruments Ltd., Worcestershire, UK).

The NP suspension was purified through centrifugation at 10,000 rpm, then the separated particles were redispersed in water, and they were further purified through a dialysis membrane. The excess ions in the solution migrate to the external aqueous solution. Afterward, to prepare the suspended solutions of Au–Co and Au NPs for injection, the colloidal solution of the particles has been mixed with 2% Tween 80, which acts as a surfactant in double distilled water (DDW) and is dispersed by ultrasonic vibration for 10 min.

**2.2. Experimental Animals, Dose Preparations, and Experimental Design.** One hundred and sixty adult male albino mice (20–25 g, purchased from the Animal House Colony, Giza, Egypt) were maintained on standard laboratory diet (protein, 16.04%; fat, 3.63%; fiber, 4.1%; and metabolic energy, 0.012 mJ) and water ad libitum at Animal House Laboratory, National Research Center, Dokki, Giza, Egypt. After an acclimation period of 1 week, animals were divided into several groups (10 mice/group) and housed individually in filter-top polycarbonate cages housed in a temperature-controlled (23 ± 1 °C) and artificially illuminated (12 h dark/light cycle) room free from any source of chemical contamination.

The genetic and biochemical evaluation of Au–Co and Au NPs have been investigated in liver tissues and bone marrow cells of male albino mice using semiquantitative RT-PCR, MN, and enzyme activity assays. According to the LD<sub>50</sub> dose of Au NPs (~3.2 g/kg bw, Hainfeld et al.<sup>26</sup>), three doses of Au–Co and Au NPs, 80, 160, and 320 mg/kg (i.e., 0.025, 0.05, and 0.1 LD<sub>50</sub>) bw, were used for genetic and biochemical evaluations. Institutional Animal Ethics Committee approved the study.

The experimental *in vivo* studies were performed on four groups. These groups were classified as negative control, positive control (cyclophosphamide), and the experimental groups including Au–Co and Au NPs. The experimental groups were divided into 3 subgroups; each one has three different doses, 80, 160, and 320 mg/kg bw. All the groups had equivalent numbers of animals per test. Thus, for gene expression, bone marrow MN, and enzyme activity assays, 10 animals were used per dose and time intervals (7 and 14 days). All animals received a single daily oral dose. The control group was treated with a DDW–Tween 80 mixture. A known mutagen, cyclophosphamide at a dose of 40 mg/kg bw was used for the positive control group. It was given intraperitoneally (i.p.), and the volume injected was 0.01 mL/g bw. The liver samples were immediately kept in liquid nitrogen, and then frozen at –80 °C prior to use for gene expression and enzyme

**Table 1.** Primers and PCR Thermo-Cycling Parameters

gene	primer sequence (5'-3')	conditions of the PCR assay	PCR amplicons (bp)
CYP3A	GAAGCATTGAGGAGGATCAC GGGTGTTGAGGGATCCAC	25 cycles: 94 °C, 40 s; 54 °C, 40 s; 72 °C, 45 s; then extension: 72 °C, 5 min	376
P53	CGCAAAGAACAGGCCACTA TCCACTCTGGGCATCCTT	25 cycles: 94 °C, 30 s; 65 °C, 30 s; 68 °C, 1 min; then extension: 68 °C, 2 min	118
P27	CAGAGGACACACACTTGGTAGA TCTTTGTTTGAGGAGAGAA	35 cycles: 93 °C, 30 s; 56 °C, 45 s; 74 °C, 45 s; then extension: 74 °C, 10 min	124
GST	CTGAACTCAGGTAGTCCAGC GGAGGTAGAAGTCACAAAG	30 cycles: 94 °C, 30 s; 55 °C, 45 s; 75 °C, 45 s; then extension: 74 °C, 10 min	329
β-actin	TTGCCGACAGGATGCAGAA GCCGATCCACACGGAGTACT	40 cycles: 94 °C, 15 s; 60 °C, 30 s; 72 °C, 1 min; then extension: 72 °C, 7 min	165

activity analyses. Bone marrow samples were collected from both femurs of each animal and extracted immediately and processed for the MN assay.

**2.3. Gene Expression Analysis.** 2.3.1. *RNA Extraction and Synthesis of First-Strand cDNA.* Immediately after killing the animals, liver tissues were kept in liquid nitrogen until gene expression analysis. Stored liver tissue samples were used to extract the total RNA [Poly(A)<sup>+</sup> RNA]. Total RNA was isolated from 100 mg of tissues by the standard TRIzol extraction method (Invitrogen, UK) and was recovered in 100 μL of molecular biology grade water. In order to remove any possible genomic DNA contamination, the total RNA samples were pretreated using DNA-free DNase treatment and a removal reagents kit (Ambion, Austin, TX, USA) following the manufacturer's protocol. The RNA concentration was determined by spectrophotometric absorption at 260 nm. To synthesize the first-strand cDNA, 5 μg of the complete Poly(A)<sup>+</sup> RNA isolated from mouse samples was reverse transcribed into cDNA in a total volume of 20 μL using 1 μL of oligo (poly(deoxythymidine)<sub>18</sub>) primer (oligo (dT) primer).<sup>27</sup> The composition of the reaction mixture consisted of 50 mM MgCl<sub>2</sub>, 10× reverse transcription (RT) buffer (50 mM KCl; 10 mM Tris-HCl; pH 8.3), 200 U/μL reverse transcriptase (RNase H free), 10 mM of each deoxyribonucleotide triphosphate (dNTP), and 50 μM oligo (dT) primer. The RT reaction was carried out at 25 °C for 10 min and raised to 42 °C for 1 h, and finished with the denaturation step at 99 °C for 5 min. Afterward, the reaction tubes containing RT preparations were flash-cooled in an ice chamber until they were used for cDNA amplification through polymerase chain reaction (PCR).<sup>28</sup>

2.3.2. *RT-PCR Assay.* The first strand cDNA from different liver tissue samples was used as the template for the semiquantitative RT-PCR with a pair of specific primers in a 25 μL reaction volume. The sequences of specific primer and product sizes are listed in Table 1. β-Actin was used as a housekeeping gene for normalizing mRNA levels of the target genes. The reaction mixture for RT-PCR consisted of 10 mM dNTP's, 50 mM MgCl<sub>2</sub>, 10× PCR buffer (50 mM KCl; 20 mM Tris-HCl; pH 8.3), 1 U/μL taq polymerase, and autoclaved water. The PCR cycling parameters of the studied genes (CYP3A, p53, p27, and GST) were performed as the PCR conditions summarized in Table 1. The PCR products were then loaded onto 2.0% agarose gel, with PCR products derived from β-actin of the different rat samples. Band intensities were measured using GeneTools analysis software (SynGen, U.K.). Each reaction of the RT-PCR was repeated with 10 mice, generating new cDNA products at least 10 times per each group.

**2.4. Micronucleus Test by Acridine Orange Fluorescent Staining.** Acridine orange staining of erythrocytes was performed by a procedure used by Ueda et al.<sup>29</sup> To assess this assay, ten animals from each treatment were sacrificed after the exposure period. The bone marrow cells were collected from both femora and resuspended in a small volume of fetal calf serum (FBS; Sigma) on a 0.003% acridine orange-coated glass slide. The slide was then covered with a cover glass to prepare bone marrow specimens. Slides were dried overnight and fixed with methanol for 10 min. Bone marrow specimens were

examined in a blind manner using fluorescence microscopy at 600× or higher magnification with a blue excitation wavelength (e.g., 488 nm) and yellow to orange barrier filter (e.g., 515 nm long pass). Two slides per animal were observed once by one observer who has sufficient experience of the micronucleus test. The number of micronucleated polychromatic erythrocytes (% MnPCEs) was measured at a rate of 3,000 polychromatic erythrocytes (PCEs) per animal.

**2.5. Determination of Enzyme Activity.** 2.5.1. *Determination of Glutathione Peroxidase Activity.* Glutathione peroxidase activity measurements were carried out by a procedure according to Miranda et al.<sup>30</sup> The reaction mixture consisted of 8 mM H<sub>2</sub>O<sub>2</sub>, 40 mM guaiacol, 50 mM sodium acetate buffer, pH 5.5, and a suitable amount of the enzyme preparation. The change in absorbance at 470 nm due to guaiacol oxidation was followed at 30 s intervals. One unit of glutathione peroxidase activity was defined as the amount of enzyme which increases the O.D. 1.0/min under standard assay conditions.

**2.6. HPLC Measurement of 8-Hydroxy-2-deoxyguanosine (8-OHdG) and 2-Deoxyguanosine (2-dG).** DNA was extracted from liver tissues by homogenization in buffer containing 1% sodium dodecyl sulfate, 10 mM Tris, 1 mM EDTA (pH 7.4), and an overnight incubation in 0.5 mg/mL proteinase K at 55 °C. Homogenates were incubated with RNase (0.1 mg/mL) at 50 °C for 10 min and extracted with chloroform/isoamyl alcohol. The extracts were mixed with 3 M sodium acetate and two volumes of 100% ethanol to precipitate DNA at -20 °C. The samples were washed twice with 70% ethanol, air-dried for 15 min, and dissolved in 100 μL of 10 mM Tris/1 mM EDTA (pH 7.4). DNA digestion was performed as previously described.<sup>31</sup> The adduct 8-OHdG was measured with high-performance liquid chromatography (HPLC) equipped with a CoulArray system (Model 5600). Analytes were detected on two coulometric array modules, each containing four electrochemical sensors attached in series, which allows identification targets based on reduction potential. UV detection was set to 260 nm. HPLC was controlled and the data acquired and analyzed using CoulArray software. The mobile phase was composed of 50 mM sodium acetate/5% methanol at pH 5.2. Electrochemical detector potentials for 8-OHdG and 2-dG were 120/230/280/420/600/750/840/900 mV, and the flow rate was 1 mL/min.

**2.7. Statistical Analysis.** All data were analyzed using the General Liner Models (GLM) procedure of Statistical Analysis System (SAS, 1982),<sup>32</sup> followed by the Scheffé-test to assess significant differences between groups. The values are expressed as the mean ± SEM. All statements of significance were based on probability of *P* < 0.05.

### 3. RESULTS

**3.1. Nanoparticle Preparation, Characterization, and Surface Modification.** The quality of the prepared NPs was ensured by measuring their optical properties and determining their particle size and shape using HRTEM. The cobalt content in situ gold particles have been confirmed by using EDX and magnetic properties measurements using VSM.

Figure 1 represents the UV-vis absorption spectra for both of Au and Au-Co bimetallic NPs. In the case of Au NPs, the

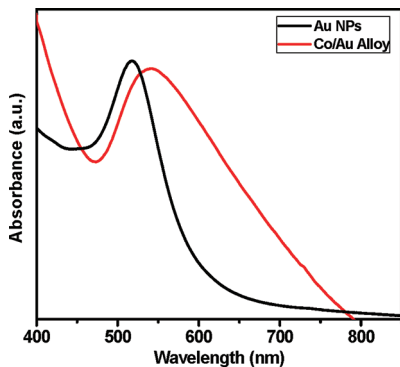


**Figure 1.** Absorption spectra of  $15 \pm 1.5$  nm pure Au (black line) and  $12 \pm 1.5$  nm Au–Co (red line) NPs.

collective oscillations of free electrons, known as the surface plasmon resonance (SPR), cause an absorption peak to appear in the visible region of the electromagnetic (EM) spectrum.<sup>33</sup> Factors that affect the position of the SPR peak have been investigated on the basis of Mie theory; for Au NPs, the SP has been shown to shift as a function of particle size, stabilizing ligand, and solvent dielectric.<sup>34</sup> On the basis of the UV–vis absorption spectra, it is clear that the spherical shape of pure Au NPs (black line) exhibits a sharp absorption band at  $\lambda_{\max} = 518$  nm owing to its SPR, while the Au–Co bimetallic NPs exhibits an absorption band (red line) with a maximum at  $\lambda_{\max} = 541$  nm and shows a broader absorption; the absorption peak broadens, covering a range from 471 to 800 nm, which is in agreement with that commonly observed in other Au bimetallic systems.<sup>34–37</sup> The red shift and broadening in SPR of Au–Co bimetallic NPs relative to the pure Au NPs reveals that the size

distribution of pure Au NPs is narrower than that of the Au–Co NPs and that the aggregation of Au–Co NPs is more serious than that of the pure Au NPs because of the induced magnetic interaction due to the presence of cobalt. Also, the homogeneous mixture of metal–metal bond between gold and cobalt leads to the formation of an intermetallic or alloyed structure, where  $\text{Co}^{2+}$  ions diffuse into the Au NP host crystal.<sup>35</sup> Templeton et al. have found that quantitatively altering pure Au cores via electronic charging caused a plasmon band shift.<sup>38</sup> Thus, the electronic properties induced by the presence of a different ( $\text{Co}^{2+}$  ions) metal may also affect plasmon band position because as Au character increases and the Co becomes buried beneath the Au, these dielectric effects may be suppressed.<sup>38</sup>

This effect was attributed to the change in the medium dielectric functions including the presence of PVP<sup>39</sup> and  $\text{Co}^{2+}$  ions, and a shortening of the electron mean free path in NPs compared to the bulk mean free path due to loss of the continuous density of states.<sup>40</sup> In addition, high iconicity of the Co matrix in which the Au nanoclusters are imbedded may further dampen the plasmon peak.<sup>41</sup>

While Schwartzberg et al.<sup>24</sup> reported that hollow gold nanospheres (HGNs) with tunable interior and exterior diameters have been synthesized by sacrificial galvanic replacement of cobalt nanoparticles, where the surface plasmon band absorption can be tuned between 550 and 820 nm by carefully controlling particle size and wall thickness. Cobalt particle size is tunable by simultaneously changing the concentration of sodium borohydride and sodium citrate, the reducing and capping agents, respectively. The thickness of the gold shell can be varied by carefully controlling the addition of gold salt.<sup>24</sup>

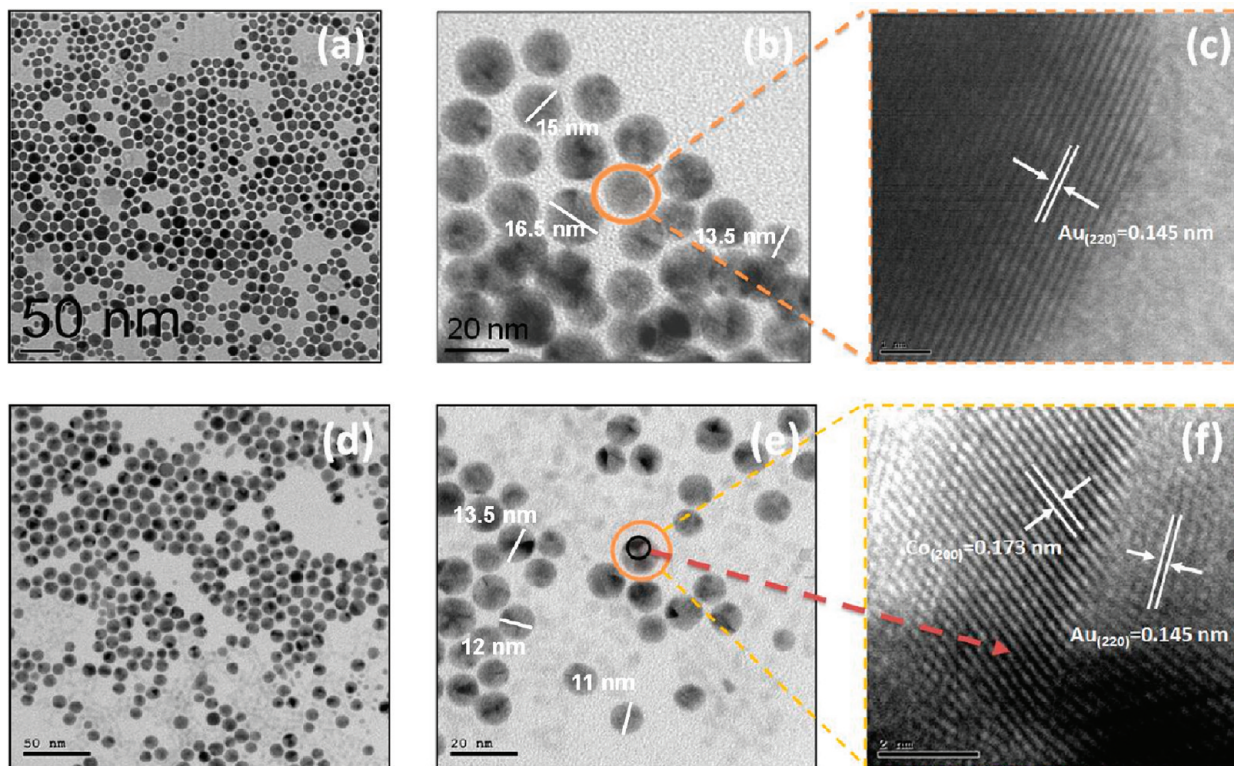


**Figure 2.** Transmission electron microscope images of  $15 \pm 1.5$  nm Au (a and b) and  $12 \pm 1.5$  nm Au–Co NPs (d and e) at different magnifications and lattice spacing of Au (c) and Au–Co nanoparticles (f).

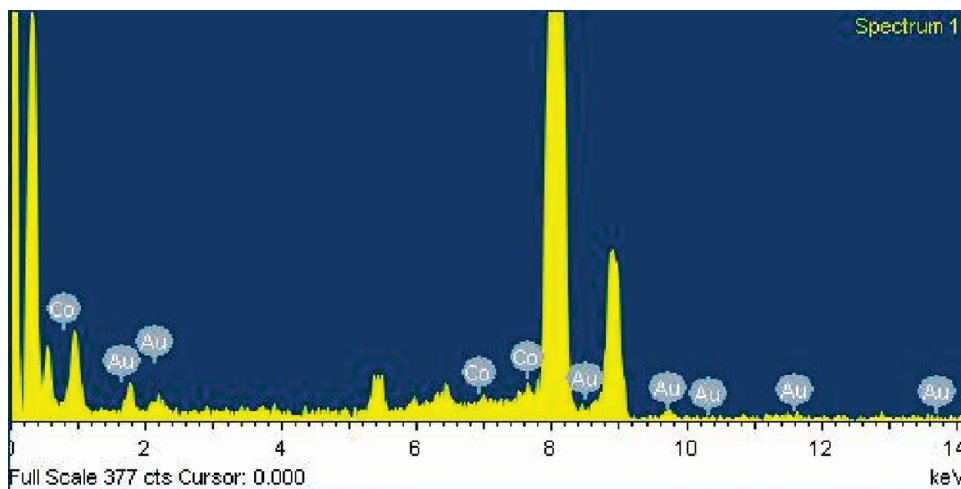


**Figure 3.** EDX spectrum shows the peaks from both Au and Co for Au–Co nanospheres and thus indicates the presence of both elements in one particle for these NPs.

Figure 2 shows the TEM images for both Au and Au–Co NPs. It is clear that the particles are of spherical-like shape with high uniformity in size and shape for both pure and Co-doped Au NPs. High-magnification imaging allows the detection of planar disorder in individual crystallites. In the case of Au NPs, the average size (diameter) was around  $15 \pm 1.5$  nm with size distribution about  $\sim 5.4\%$  rms (Figure 2a, and b), while in the case of Au–Co NPs, the size is about  $12 \pm 1.5$  nm for Co-doped Au NPs with size distribution about  $\sim 6.7\%$  rms (Figure 2d and e). The presence of cobalt in the gold nanocrystal induces defects due to the lattice mismatch and also introduces magnetic properties to the gold spheres. HRTEM images, as illustrated in Figure (2f), show a break in symmetry within the gold crystal lattice due to the existence and diffusion of cobalt atoms through the gold lattice at the metal–metal interface. In the lattice image at a concentration of  $1 \times 10^{-3}$  M of  $\text{Co}^{2+}$  ions, the  $d$ -spacings are 0.145 and 0.173 nm, which are in agreement with the planar distance of Au [220] (0.144 nm) and Co [200] (0.178 nm), respectively (Figure 2c, and 2f).

Typical EDX study performed during the imaging of the spheres confirms the presence of Au and Co as shown in Figure 3. The element mappings show that Co and Au are homogeneously mixed in the spheres, indicating the diffusion of  $\text{Co}^{2+}$  ions in situ Au particles, and verify the formation of an alloy. The spectrum shows peaks at 1.6, 2, and 9 MeV that correspond to Au, and a peak at 7.0 and 7.6 MeV which corresponds to Co, suggesting that the NPs have a Au–Co bimetallic structure. The line profiles of composition also verify the lower percentage of  $\text{Co}^{2+}$  ions into  $\text{Au}^0$  nanospheres; they are listed in Table 2 and illustrated in Figure 2. It is clear that the cobalt and gold contents are an average of about 36.39 and 63.61 wt %, respectively (Table 2). This is a significant indication for the doping and diffusion of  $\text{Co}^{2+}$  ions and thus the formation of an alloy. Boyer et al.<sup>41</sup> reported the synthesis

of inhomogeneous bimetallic nanoparticles with an average diameter of 11 nm consisting of nanoclusters fabricated by pulsed laser processes, where the EDX data showed that the produced bimetallic nanoparticles consisted of 68% Co and 32% Au.<sup>41</sup>

Dynamic light scattering (DLS) and electrophoretic mobility for as-prepared samples suspended in both DDW and a mixture of 98% DDW+2% Tween 80 are represented in Table 3. We

**Table 3. DLS Data of the Au NPs and Au–Co NPs**

vehicles	diameter (nm) HD <sup>a</sup>	poly dispersity index	zeta potential (mV)	surface	medium	pH
Au NPs	$31.0 \pm 1.8$	0.054	-26.8	PVP	DDW <sup>b</sup>	6.23
	$33.0 \pm 1.2$	0.061	-35.7		DDW +TW 80 <sup>c</sup>	5.35
Au–Co NPs	$29.4 \pm 0.5$	0.067	-30.3		DDW <sup>b</sup>	6.20
	$31.7 \pm 1.1$	0.078	-37.1		DDW +TW 80 <sup>c</sup>	5.30

<sup>a</sup>HD is hydrodynamic diameter. <sup>b</sup>DDW is double distilled water.

<sup>c</sup>TW80 is Tween 80.

measured the size and zeta potential in a vehicle, for both Au and Au–Co NPs as listed in Table 3. In the case of suspension into DDW as a solvent, the pure Au NPs have a hydrodynamic diameter (HD) of approximately  $31 \pm 1.8$ , and  $29.4 \pm 0.5$  nm for Au–Co NPs. The polydispersity indices for Au and Au–Co are 0.054 and 0.067, respectively, depending on the vehicle. Both Au and Au–Co have a negative zeta potential in all tested vehicles, but the Au–Co NPs are 1.33-fold more negative than the Au NPs (Table 3). This is due to the formation of secondary size from cobalt nanoclusters in Au–Co NPs. While in the case of suspension into a mixture of 98% DDW + 2% Tween 80 as a solvent, the pure Au NPs have a HD of approximately  $33 \pm 1.2$  and  $31.7 \pm 1.1$  nm for Au–Co NPs. The polydispersity indices for Au and Au–Co are 0.061 and 0.078, respectively, depending on the vehicle. Both Au and Au–Co have a negative zeta potential in all tested vehicles, but the Au–Co NPs are 1.2-fold more negative than the Au NPs (Table 3). This is due to the formation of secondary size from cobalt nanoclusters in Au–Co NPs.

**Table 2. EDX Quantitative Analysis (the Chemical Composition) of Single Au–Co NPs**

element	peak area	area sigma	k-factor	Abs corr.	weight %
Co K	35	39	2.632	1.000	36.39
Au M	111	50	1.458	1.000	63.61
totals					100.00

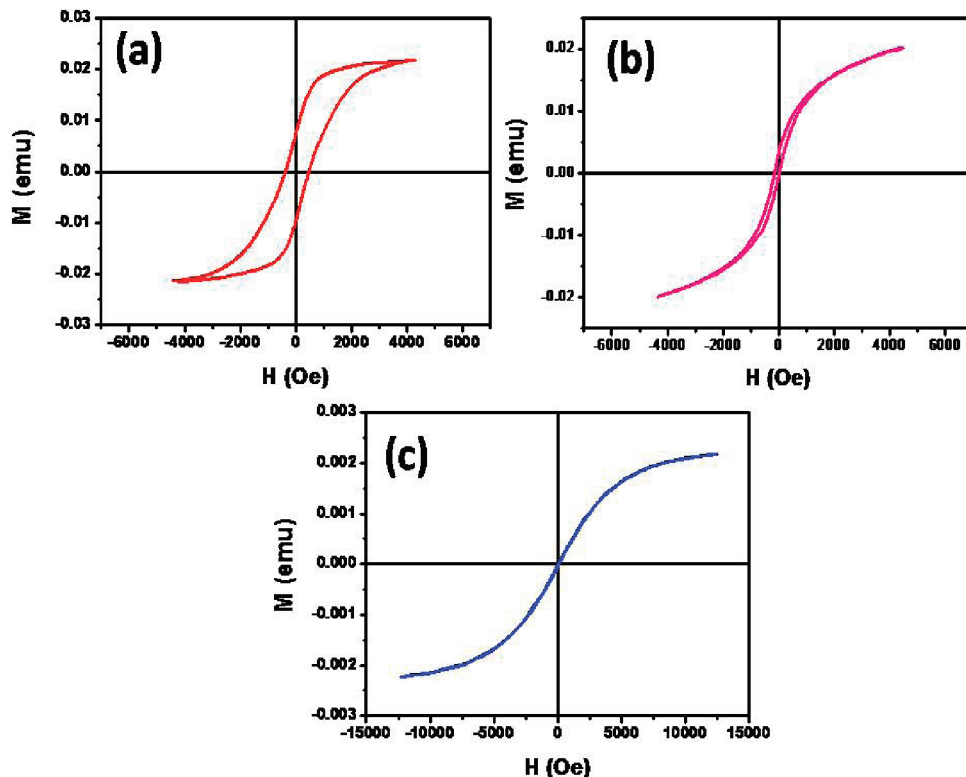


**Figure 4.** Room temperature hysteresis loop of Au–Co nanoparticles with an average size of 50 nm (a), 25 nm (b), and 12 nm (c).

Figure 4a, b, and c shows the magnetic property analysis of the Au–Co NPs with size variations between 10 to 50 nm. Figure 4a shows the magnetic properties of Au–Co with average size around 50 nm. Figure 4b and c shows that the average size of the nanoparticles decreased to 25 and 12 nm, respectively. The hysteresis loop shows ferromagnetic behavior due to the existence  $\text{Co}^{2+}$  ions inside the gold particles. It is clear that the hysteresis loops of the Figure 4a, b, and c have different switching fields and magnetic moments based on the average size of the Au–Co NPs. From Figure 4, it is clear that the decrease in the particle size leads to a decrease in switching field and magnetic moment. This finding can be attributed to the presence of the Co element with decreasing amounts as the size of the Au–Co NPs decreases. The magnetic properties of the Au–Co nanoparticles with 12 nm size show superparamagnetic behavior, which is suitable for biomedical applications, which is why 12 nm particles have been chosen in this study.

**3.2. Gene Expression.** Expression of tumor-initiating (CYP3A, p53, and p27) and antioxidant (GST) genes in the liver of male mice exposed to Au–Co and Au NPs have been summarized in Figures 5–8. Regarding tumor-initiating genes, the current results revealed a significant increase in the hepatic mRNA level of mice exposed to Au–Co NPs (Figures 5–7). Exposure to Au–Co NPs with doses of 160 and 320 mg/kg bw for 14 days significantly increased the expression of CYP3A and p27 gene (Figures 5 and 7). Moreover, the highest dose of Au–Co NPs for 7 and 14 days significantly increased the expression level of p53 gene (Figure 6). However, the low dose of Au–Co NPs did not significantly increase the expression levels of CYP3A, p53, and p27 genes at both time intervals (Figures 5–7). However, exposure of male mice to Au NPs with the highest dose significantly increased the expression levels of

CYP3A, p53, and p27 genes especially at the 14th day of treatment (Figures 5–7). However, the low and medium doses of Au NPs at 7 and 14 days did not significantly increase the levels of CYP3A, p53, and p27 genes in mouse liver tissues (Figures 5–7).

Evaluation of the antioxidant gene (GST) expression revealed that exposure to Au–Co NPs had significantly decreased the expression level with the medium and the highest dose at the 14th day after treatment (Figure 8). However, the 80 and 160 mg/kg bw doses of Au–Co NPs did not significantly decrease the expression levels of GST gene at the seventh day after treatment (Figure 8). Exposure of male mice to Au NPs with the highest dose (320 mg/kg bw) decreased significantly the expression level of the GST gene at the 14th day after treatment (Figure 8). In contrast, exposure of male mice to Au NPs with low and medium doses at 7 and 14 days did not significantly decrease the levels of the GST gene (Figure 8). Nearly the same results were obtained when the PCR assay was performed for each individual sample within each group (10 animals).

**3.3. Micronucleus Assay.** Effect of Au–Co and Au NPs on MnPCE formation in the bone marrow cells of male mice is summarized in Figure 9. The results showed that the low dose of Au–Co NPs did not significantly increase the incidence of MnPCEs at both time intervals in comparison to that in the control group (Figure 9). However, exposure of male mice with the medium and high doses of Au–Co NPs at the 7th and 14th days after treatment significantly increased the incidence of MnPCEs ( $9.7 \pm 0.1$  and  $12.6 \pm 0.2$ ;  $10.7 \pm 0.1$  and  $13.9 \pm 0.2$  for 160 and 320 mg/kg bw, respectively) compared with that in the control group ( $5.3 \pm 0.1$  and  $5.9 \pm 0.1$ , respectively; Figure 9). However, treatment of male mice with low and medium doses of Au NPs increased MnPCE formation in the bone

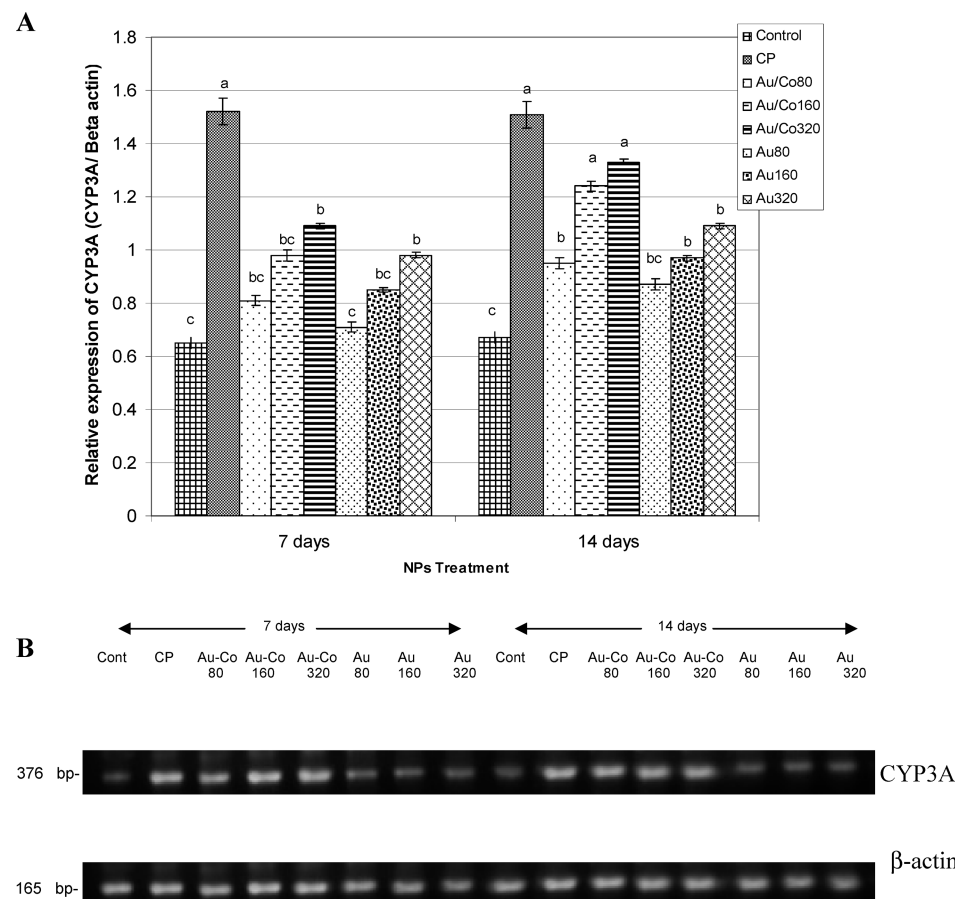


**Figure 5.** Expression of CYP3A gene in the liver of mice exposed to Au–Co and Au NPs determined by semiquantitative RT-PCR (A and B). The RNA recovery rate was estimated as the ratio between the intensity of CYP3A gene and the  $\beta$ -actin gene. Mean values within tissues with unlike lowercase letters (a, b, and c) were significantly different ( $P < 0.05$ , Scheffé-test), while mean values within tissues with similar lowercase letters (a, b, and bc) were not significantly different ( $P > 0.05$ ).

marrow cells at both time intervals without significant differences (Figure 9). However, the high dose of Au NPs was able to significantly increase the incidence of MnPCEs in the bone marrow cells at both time intervals ( $9.8 \pm 0.2$  and  $11.1 \pm 0.1$ , respectively) in comparison with that in the control group ( $5.3 \pm 0.1$  and  $5.9 \pm 0.1$ , respectively; Figure 9).

**3.4. Determination of Glutathione Peroxidase Activity.** The present study showed that male mice exposed to Au-

**ity.** The present study showed that male mice exposed to Au–Co NPs with doses of 160 and 320 mg/kg bw at both time intervals represented significantly low levels of the glutathione peroxidase activity compared to that of the control group (Table 4). Along the same trend, male mice exposed to Au NPs with the highest dose at both time intervals showed significantly low levels of the glutathione peroxidase activity compared to that of the control group (Table 4). However, male mice exposed to Au NPs with low and medium doses at both time intervals showed relatively similar levels of enzyme activity to those of the control group (Table 4).

### 3.5. Generation of 8-Hydroxy-2-deoxyguanosine (8-

**OHDG).** Assessment of 8-OHDG generation in the hepatic mice genome following Au- and Au-Co NP treatment as a surrogate for oxidative stress induced damage is summarized in Figure 10. The current results indicated that 8-OHDG levels in control liver tissues ranged from 3.6 8-OHDG per  $10^5$  dG to 3.5 8-OHDG per  $10^5$  dG (Figure 10a and b).

The 8-OHdG/2-dG ratio following a low dose of Au NP treatment at 7 and 14 days was relatively similar to that of the

control group. However, the ratio of 8-OHDG/2-dG generation increased to 1.5-fold following a medium dose of Au NPs at 14 days after treatment in comparison to that of the control group. In addition, this ratio increased from 1.4-fold at 7 days to 2.6-fold at 14 days after Au NPs treatment (Figure 10a and b).

Along the same trend, the ratio of 8-OHdG/2-dG generation increased slightly following a low dose of Au–Co NPs treatment at 7 and 14 days compared with that in the control group (Figure 10a and b). However, the ratio of 8-OHdG/2-dG generation increased to 1.5- and 2.2-fold at 7 days to 3.1- and 3.6-fold at 14 days following medium and high doses of Au–Co NPs treatment, respectively (Figure 10a and b).

## 4. DISCUSSION

In an attempt to characterize the potential toxicity of Au NPs in therapeutic or diagnostic use, we investigated changes in hepatic RNA expression, hepatic enzyme levels, genomic damage caused by oxidative stress (8-OHdG), and micronuclei (MNs) formation in bone marrow following a single oral administration of PVP-capped Au or Au-Co alloy nanoparticles over a two week period. The current results indicated time- and dose-dependent up-regulation of CYP3A and down-regulation of GST (genes involved in drug metabolism), as well as up-regulation of p53 and p27 (genes involved in cell cycle regulation) in liver tissues exposed to Au and Au-Co nanoparticles. The observations of micronuclei formation in bone marrow cells and generation of DNA adduct (8-OHdG)

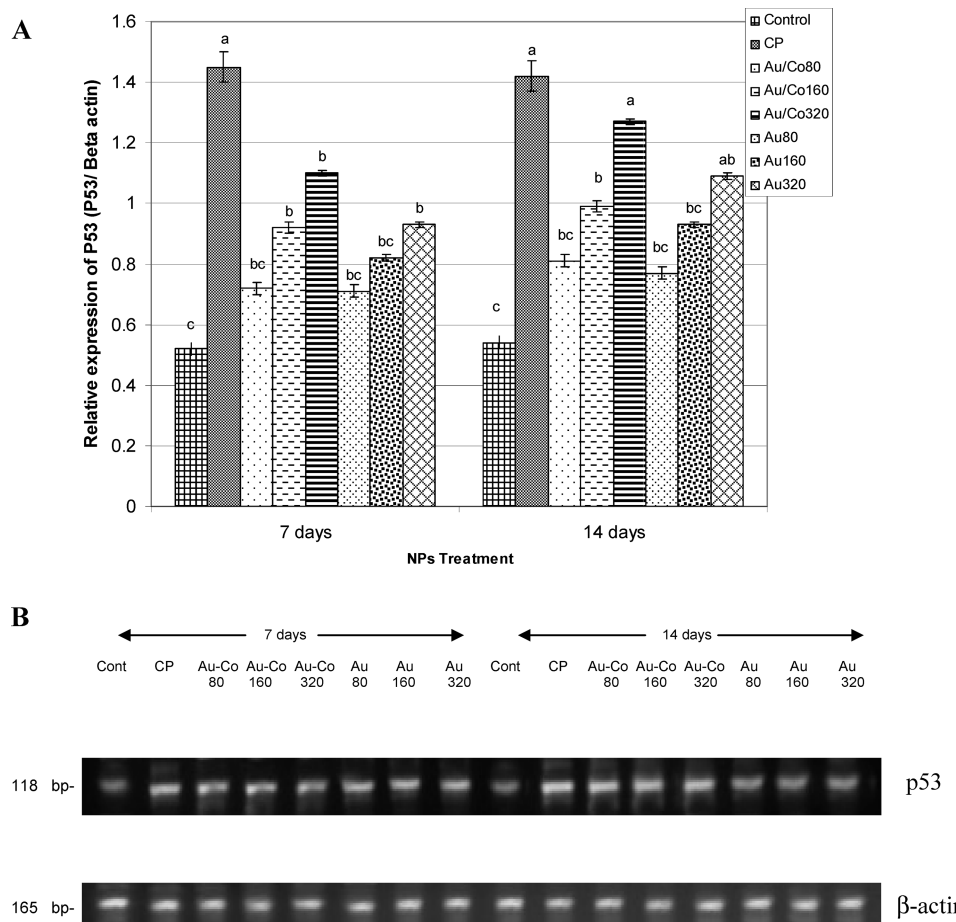


**Figure 6.** Expression of p53 gene in the liver of mice exposed to Au–Co and Au NPs determined by semiquantitative RT-PCR (a and b). The RNA recovery rate was estimated as the ratio between the intensity of p53 gene and the  $\beta$ -actin gene. Mean values within tissues with unlike lowercase letters (a, b, and c) were significantly different ( $P < 0.05$ , Scheffé-test), while mean values within tissues with similar lowercase letters (a, b, and bc) were not significantly different ( $P > 0.05$ ).

were significantly augmented with increasing dosage and time following exposure to both particles.

Our results are consistent with Balasubramanian et al.,<sup>42</sup> who found that several genes were altered in the liver after Au NP treatment. They found also that the greatest increase of the expression was found with cytochrome P450. In addition, several other members of the cytochrome P450 family, including members of CYP4a and CYP3, were significantly up-regulated after Au NPs injection. These findings suggested that toxic metabolic genes/pathways are induced when mice are exposed to Au NPs as stated in the current study. Cytochrome P450s are localized in the inner membrane of mitochondria or the endoplasmic reticulum of cells and catalyze multiple reactions, which accounts for their central importance in metabolism and detoxification of extremely large numbers of endogenous and exogenous molecules. In the liver, these substrates include metabolic products, drugs, and toxic compounds, which play a direct or indirect role in the alteration of the metabolic genes/pathways existing in those tissues.

Regarding the expression changes of the genes involved in cell cycle regulation in relation to Au NP treatment, Cho et al.<sup>43</sup> investigated the gene expression profiles in mouse liver following a single intravenous injection of PEG-coated Au NPs. They found that commonly expressed genes were categorized as cell cycle, apoptosis, inflammation, and

metabolic processes. Such findings are consistent with our results, which found up-regulation of cell cycle regulation genes (p53 and p27) in liver tissues exposed to Au and Au–Co NPs.

An explanation for the reason that Au NPs cause alterations in the gene expression in liver tissues is cited in numerous studies.<sup>42–45</sup> They reported that injection of different sizes of Au NPs in rats resulted in accumulation mainly in the liver.<sup>42–44</sup> In addition, Garnett and Kallinteri<sup>45</sup> reported that organs of the reticuloendothelial system (RES) including the liver and spleen can efficiently accumulate NPs via opsonization; that is, NPs could bind to antibodies in the plasma and are subsequently recognized by the phagocyte-rich RES. This may explain the persistent accumulation of Au NPs in hepatic cells caused by gene expression changes.

The current study found that Au–Co NPs were able more than Au NPs to induce significant alteration in the tumor-initiating genes associated with an increase of MN formation and a reduction in glutathione peroxidase activity. Although, Au NPs are recognized by Cho et al.<sup>46</sup> as being as nontoxic, there are some reports on their toxicity, which indicate that the toxicity depends on the physical dimension, coating bioactivity, surface chemistry, and shape of the nanoparticles. Therefore, increase in the toxicity due to Au–Co NP treatment in the present work may be attributed to the presence of cobalt in the alloy. The fact that the Au–Co nanoalloy induces more toxicity than pure Au NPs may be due to the exposure of the NPs to

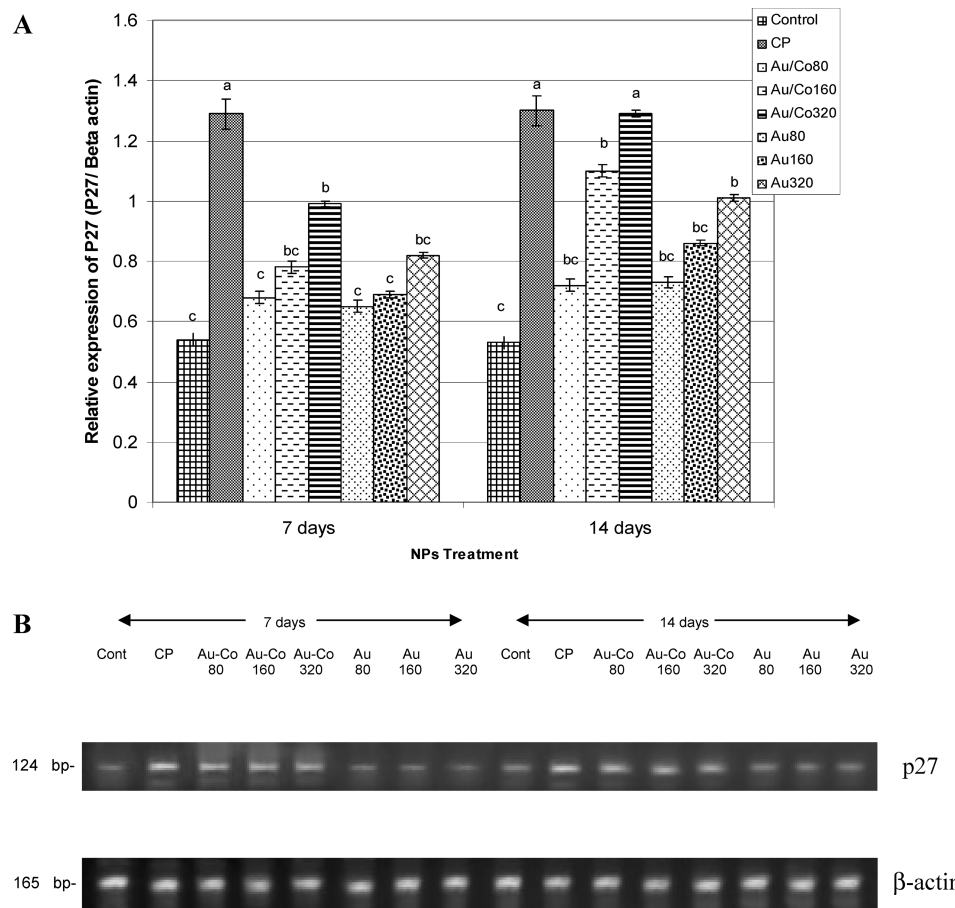


**Figure 7.** Expression of p27 gene in the liver of mice exposed to Au–Co and Au NPs determined by semiquantitative RT-PCR (a and b). The RNA recovery rate was estimated as the ratio between the intensity of p27 gene and the  $\beta$ -actin gene. Mean values within tissue with unlike lowercase letters (a, b, and c) were significantly different ( $P < 0.05$ , Scheffé-test), while mean values within tissues with similar lowercase letters (a, b, and bc) were not significantly different ( $P > 0.05$ ).

low pH. Our previous study<sup>47</sup> reported that oral administration of nanoparticles tends to cause agglomeration when they are suspended in a low pH liquid producing an alteration of their surface ionic composition. This might cause the nanoparticles to separate from their agglomerates and produce an increased surface area, potentially increasing the generation of a cellular ROS. In the present study, the Au–Co NPs were exposed to low pH because they were administered orally to the male mice and then passed to the gastric tract. Therefore, Au–Co NPs may be degraded, and their coating molecules are damaged between 7 to 14 days of treatment. Consequently, it may be presumed that induction of MnPCE formation, DNA damage, and generation of high amounts of 8-OHdG were probably caused by the alteration of Au–Co NPs surface ionic composition and/or high intracellular ROS generation. Our results are in agreement with those of Colognato et al.,<sup>12</sup> who demonstrated that Co NPs were capable of inducing clastogenicity in human peripheral blood leukocytes and that this was accompanied by reducing cell viability. In addition, cobalt ions were able to produce single strand breaks, chromosomal aberrations, and sister-chromatid exchanges in human MCF-7 cells.<sup>13,14</sup> Moreover, Zhu et al.<sup>48</sup> reported that cobalt chloride was able to induce apoptosis of RGC-5 cells and increase the expression of the tumor-initiating P53 gene.

A key mechanism thought to be responsible for the genetic alterations exerted by Co NPs involves oxidative stress, which

refers to a redox imbalance within cells usually as a result of increased intracellular reactive oxygen species (ROS) and decreased antioxidants.<sup>49</sup>

Further explanation to express the effect of Co NP induced toxicity was thought to be due to the release of  $\text{Co}^{2+}$  ions from the Co NPs.<sup>17</sup> These ions increase ROS release with their potential enhanced generation of 8-OHdG induced DNA damage and alterations in gene expression. Moreover, Singh et al.<sup>49</sup> demonstrated that  $\text{Co}^{2+}$  ions released from certain nanoparticles can cause the conversion of cellular oxygen metabolic products such as  $\text{H}_2\text{O}_2$  and superoxide anions to OH. The hydroxyl radical represents one of the primary DNA damaging species, which can diffuse through the cellular and nuclear membrane and thus can cause thymine–tyrosine (DNA–histone protein) cross-links in chromatin.<sup>50</sup> Furthermore, free metal ions can result in OH-induced purine and pyrimidine modifications.<sup>51</sup> We found good agreement between the previous findings and our results, where Au–Co NPs inhibit the antioxidant activity of the glutathione peroxidase enzyme and down-regulate the expression of GST gene.

Although, the results of our study show that Au NPs were less toxic than Au–Co NPs, only the highest dose of Au NPs was able to increase the expression changes of CYP3A, p53, and p27 genes, MN formation, and generation of DNA adduct. Our results are consistent with several studies which reported that neutral Au NPs caused DNA damage and increased both

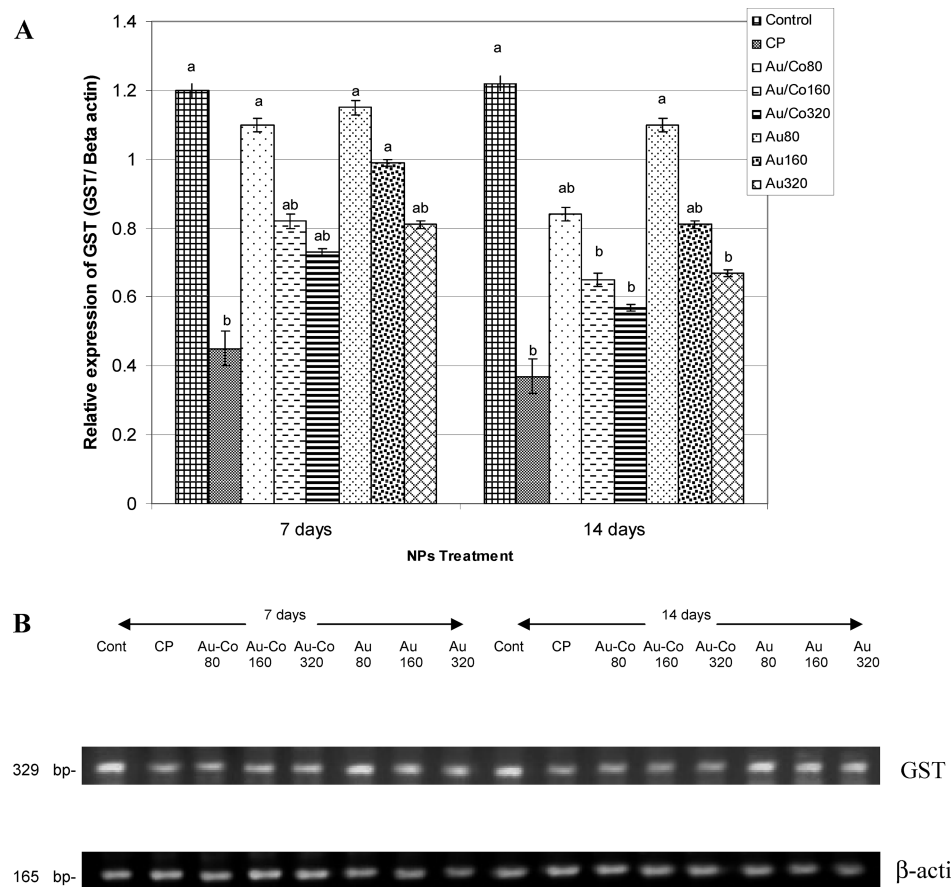


**Figure 8.** Expression of GST gene in the liver of mice exposed to Au–Co and Au NPs determined by semiquantitative RT-PCR (a and b). The RNA recovery rate was estimated as the ratio between the intensity of GST gene and the  $\beta$ -actin gene. Mean values within tissues with unlike lowercase letters (a, b, and c) were significantly different ( $P < 0.05$ , Scheffé-test), while mean values within tissues with similar lowercase letters (a, b, and bc) were not significantly different ( $P > 0.05$ ).

nuclear and cytoplasmic p53 expression in a human keratinocyte cell line (HaCaT).<sup>52,53</sup>

Numerous studies attempted to explain the regulation of gene/enzyme changes and genetic toxicity including micronuclei formation in relation to Au NP treatment. Johnston et al.<sup>54</sup> reported that Au NPs are recognized for their ability to bind to DNA, which may be exploited within the treatment of diseases but may also contribute to genotoxicity or affect gene expression (block transcription). Molecular simulations and TEM analyses were used to determine the ability of Au NPs to interact with DNA molecules.<sup>55</sup> Tsoli et al.<sup>56</sup> found that Au NPs were able to traverse the plasma membrane and subsequently distribute subcellularly. It was revealed that Au NPs were distributed within the cytoplasm and nucleus, where they were capable of binding to DNA. This finding therefore not only confirmed that NPs were strongly bound to DNA but also demonstrated their cytotoxic potential. In addition, Goodman et al.<sup>57</sup> illustrated the ability of Au NPs to bind to DNA, which caused a conformational change within the structure of DNA. This was suggested to impact DNA transcription and was exemplified by the finding that RNA polymerase activity was inhibited as well as subsequent enzymes level changes. The interaction of Au NPs with serum proteins is likely to enable their transportation within the body. In addition, interactions with proteins may have detrimental consequences for particle behavior or normal protein structure and function, and therefore impact normal

cell function, especially antioxidant defense. Furthermore, the ability of Au NPs to interrupt transcription and translation is of concern.

However, hepatic cells are able to detoxify a variety of substances often accompanied by ROS formation<sup>58</sup> and also have potential defense mechanisms, including intracellular antioxidants and antioxidant enzymes such as glutathione peroxidase, superoxide dismutase, and catalase.<sup>59</sup> These observations are in agreement with the current results, where mouse hepatic cells exposed to Au NPs in the present study could not decrease the level of the antioxidant glutathione peroxidase enzyme except the highest dose of Au NPs (320 mg/kg bw). Therefore, it would appear that the ROS levels caused by Au NP exposure concentrations used in our study were not high enough to overcome antioxidant defense mechanisms and thus cause immediate gene expression alterations and MN formation. Further experiments will be needed to determine other likely long-term effects, such as DNA damage, that are known to be caused by elevated ROS production.

## 5. CONCLUSIONS

We report that the Au–Co alloy NPs caused more alterations in gene expression, DNA damage (MNs), and DNA adduct than Au NPs. These influences were accompanied by reduction in antioxidant defense and may consequently cause an increase in ROS formation which induce gene expression alterations and

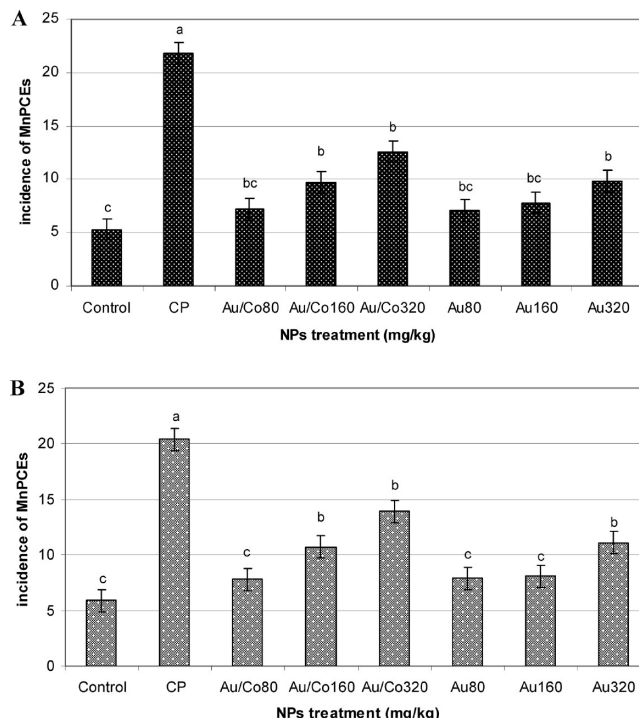


**Figure 9.** Micronucleated polychromatic erythrocytes (MnPCEs) of male mice exposed to Au–Co and Au NPs at 7 (a) and 14 days (b). Results are expressed as the mean  $\pm$  SEM of data from at least 10 samples. Mean values within tissues with unlike lowercase letters (a, b, and c) were significantly different ( $P < 0.05$ , Scheffé-test), while mean values within tissues with similar lowercase letters (b and c) were not significantly different ( $P > 0.05$ ). CP, cyclophosphamide; Co, cobalt; Au, gold; NPs, nanoparticles.

**Table 4. Amount of Glutathione Peroxidase Activity in Mice Exposed to Au–Co and Au NPs (mg/kg) at Several Time Intervals<sup>a</sup>**

treatment <sup>b</sup>	glutathione peroxidase activity (U/mg tissues/min)	
	7 days <sup>c</sup>	14 days <sup>c</sup>
control	5.7 $\pm$ 0.03 a	5.5 $\pm$ 0.03 a
cyclophosphamide	1.6 $\pm$ 0.10 c	1.4 $\pm$ 0.10 c
Au–Co-80	5.2 $\pm$ 0.14 ab	4.1 $\pm$ 0.14 ab
Au–Co-160	3.7 $\pm$ 0.13 b	3.0 $\pm$ 0.13 b
Au–Co-320	3.2 $\pm$ 0.11 b	2.8 $\pm$ 0.11 b
Au-80	5.4 $\pm$ 0.12 ab	4.5 $\pm$ 0.12 ab
Au-160	4.6 $\pm$ 0.11 ab	4.3 $\pm$ 0.11 ab
Au-320	4.0 $\pm$ 0.12 b	3.2 $\pm$ 0.12 b

<sup>a</sup>Mean values within tissue with unlike lowercase letters were significantly different ( $P < 0.05$ , Scheffé-test), while mean values within tissues with similar lowercase letters were not significantly different ( $P > 0.05$ ). <sup>b</sup>Each treatment had equivalent numbers of animals ( $n = 10$ ). <sup>c</sup>Time of sample collection after treatment.

genetic toxicity. However, Au NPs could not induce this toxicity in DNA that was accompanied by a level of the antioxidant glutathione peroxidase enzyme similar to that of the control group except for the highest dose. Therefore, it would appear that ROS levels caused by Au NP exposure were not high enough to overcome antioxidant defense mechanisms. These results might be useful for designing NPs for biomedical applications such as cancer therapy and imaging, drug delivery, and smart targeting.

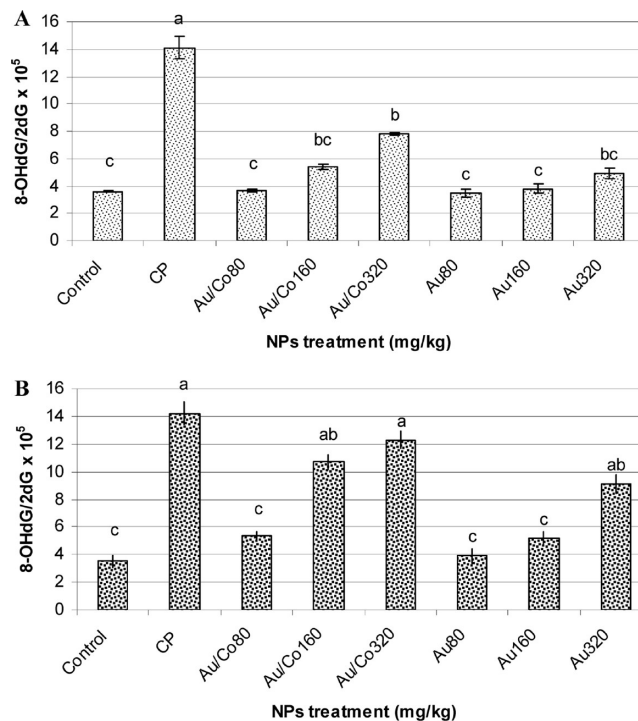


**Figure 10.** Generation of 8-OHdG in the hepatic mice genome following Au- and Au–Co NPs at 7 (a), and 14 days (b). DNA damage was expressed as the ratio of oxidized DNA base (8-OHdG) to nonoxidized base (2-dG) in liver DNA. Results are expressed as the mean  $\pm$  SEM of data from at least 10 samples. Mean values within tissues with unlike lowercase letters (a, b, and c) were significantly different ( $P < 0.05$ , Scheffé-test). Mean values within tissues with similar lowercase letters (ab and bc) were not significantly different ( $P > 0.05$ ). CP, cyclophosphamide.

## ■ AUTHOR INFORMATION

### Corresponding Author

\*Advanced Materials and Nanotechnology Lab, CEAS National Research Centre (NRC) El-Behouth Street, 12622 Dokki, Giza, Egypt. Phone: (+202) 0126027416. Fax: (+202) 33370931. E-mail: egirgis@gmail.com.

### Funding

This study was supported by Swedish research foundation SIDA under grant # 348-2007-6992 and Egyptian fund from STDF project ID# 1885.

### Notes

The authors declare no competing financial interest.

## ■ ACKNOWLEDGMENTS

We thank all our colleagues in Animal House, National Research Centre, Dokki, Giza, for taking care of the animals throughout the experiments.

## ■ REFERENCES

- (1) ASTM International (2006) ASTME 2456-06, Terminology for Nanotechnology, available at <http://www.astm.org>.
- (2) Niemeyer, C. M. (2001) Nanoparticles, proteins, and nucleic acids: biotechnology meets materials science. *Angew. Chem., Int. Ed.* 40, 4128–4158.
- (3) Christian, P., Von der Kammer, F., Baalousha, M., and Hofmann, T. (2008) Nanoparticles: structure, properties, preparation and behavior in environmental media. *Ecotoxicology* 17, 326–343.

- (4) Nel, A., Xia, T., Madler, L., and Li, N. (2006) Toxic potential of materials at the nanolevel. *Science* 311, 622–627.
- (5) Chitrani, B. D., Ghazani, A. A., and Chan, W. C. W. (2006) Determining the size and shape dependence of gold nanoparticle uptake into mammalian cells. *Nano Lett.* 6, 662–668.
- (6) Azzay, H. M. E., and Mansour, M. M. H. (2009) In vitro diagnostic prospects of nanoparticles. *Clin. Chim. Acta* 403, 1–8.
- (7) Yih, T. C., and Al-Fandi, M. (2006) Engineered nanoparticles as precise drug delivery systems. *J. Cell. Biochem.* 97, 1184–1190.
- (8) Pan, Y., Neuss, S., Leifert, A., Fischler, M., Wen, F., Simon, U., Schmid, G., Brandau, W., and Jahnens-Dechent, W. (2007) Size-dependent cytotoxicity of gold nanoparticles. *Small* 3, 1941–1949.
- (9) Connor, E. E., Mwamuka, J., Gole, A., Murphy, C. J., and Wyatt, M. D. (2005) Gold nanoparticles are taken up by human cells but do not cause acute cytotoxicity. *Small* 1, 325–327.
- (10) Pernodet, N., Fang, X., Sun, Y., Bakthina, A., Ramakrishnan, A., Sokolov, J., Ulman, A., and Rafailovich, M. (2006) Adverse effects of citrate/gold nanoparticles on human dermal fibroblasts. *Small* 2, 766–773.
- (11) Tedesco, S., Doyle, H., Redmond, G., and Sheehan, D. (2008) Gold nanoparticles and oxidative stress in *Mytilus edulis*. *Mar. Environ. Res.* 66, 131–133.
- (12) Colognato, R., Bonelli, A., Ponti, J., Farina, M., Bergamaschi, E., and Sabbioni, E. (2008) et al. Comparative genotoxicity of cobalt nanoparticles and ions on human peripheral leukocytes in vitro. *Mutagenesis* 23, 377–382.
- (13) Baldwin, E. L., Byl, J. A., and Osheroff, N. (2004) Cobalt enhances DNA cleavage mediated by human topoisomerase II alpha *in vitro* and in cultured cells. *Biochemistry* 43, 728–735.
- (14) Kopera, E., Schwerdtle, T., Hartwig, A., and Bal, W. (2004) Co(II) and Cd(II) substitute for Zn(II) in the zinc finger derived from the DNA repair protein XPA, demonstrating a variety of potential mechanisms of toxicity. *Chem. Res. Toxicol.* 17, 1452–1458.
- (15) Cirla, A. M. (1994) Cobalt-related asthma: clinical and immunological aspects. *Sci. Total Environ.* 150, 85–94.
- (16) Lison, D., Lauwers, R., Demedts, M., and Nemery, B. (2004) Experimental research into the pathogenesis of cobalt/hard metal lung disease. *Eur. Respir. J.* 9, 1024–1028.
- (17) Peters, K., Unger, R. E., Kirkpatrick, C. J., Gatti, A. M., and Monari, E. (2004) Effects of nano-scaled particles on endothelial cell function *in vitro*: studies on viability, proliferation and inflammation. *J. Mater. Sci. Mater. Med.* 15, 321–325.
- (18) Mayer, A. B. R., and Mark, J. E. (1998) Colloidal gold nanoparticles protected by water-soluble homopolymers and random copolymers. *Eur. Polym. J.* 34, 103–108.
- (19) Male, K. B., Li, J., Bun, C. C., Ng, S., and Luong, J. H. T. (2008) Synthesis and stability of fluorescent gold nanoparticles by sodium borohydride in the presence of mono-6-deoxy-6-pyridinium- $\alpha$ -cyclodextrin chloride. *J. Phys. Chem. C* 112, 443–451.
- (20) Martin, M. N., Basham, J. I., Chando, P., and Eah, S.-K. (2010) Charged gold nanoparticles in non-polar solvents: 10-min synthesis and 2D self-assembly. *Langmuir* 26, 7410–7417.
- (21) McFarland, A. D., Haynes, C. L., Mirkin, C. A., Van Duyne, R. P., and Godwin, H. A. (2004) Color my nanoworld. *J. Chem. Educ.* 81, S44A.
- (22) Lisicki, I. (2004) Size control of spherical metallic nanocrystals. *Colloids and Surf., A* 250, 499–507.
- (23) Chen, G., Takezawa, M., Kawazoe, N., and Tateishi, T. (2008) Preparation of cationic gold nanoparticles for gene delivery. *Open Biotech. J.* 2, 152–156.
- (24) Schwartzberg, A. M., Olson, T. Y., Talley, C. E., and Zhang, J. Z. (2006) Synthesis, characterization, and tunable optical properties of hollow gold nanospheres. *J. Phys. Chem. B* 110, 19935–19944.
- (25) Haiss, W., Thanh, N. T. K., Aveyard, J., and Fernig, D. G. (2007) Determination of size and concentration of gold nanoparticles from UV-vis spectra. *Anal. Chem.* 79, 4215–4221.
- (26) Hainfeld, J. F., Slatkin, D. N., Focella, T. M., and Smilowitz, H. M. (2007) Gold nanoparticles: a new X-ray contrast agent. *Br. J. Radiol.* 80, 64–65.
- (27) El- Makawy, A., Girgis, S. M., and Khalil, W. K. B. (2008) Developmental and genetic toxicity of stannous chloride in mouse dams and fetuses. *Mutat. Res.* 657, 105–110.
- (28) Khalil, W. K. B., and Booles, H. F. (2011) Protective role of selenium against over-expression of cancer-related apoptotic genes induced by o-cresol in rats. *Arch. Hig. Rada. Toksykol.* 62, 121–129.
- (29) Ueda, T., Hayashi, M., Koide, N., Sofuni, T., and Kobayashi, J. (1992) A preliminary study of the micronucleus test by acridine orange fluorescent staining compared with chromosomal aberration test using fish erythropoietic and embryonic cells. *Water Sci. Technol.* 25, 235–240.
- (30) Miranda, M. V., Fernandez Lahor, H. M., and Cascone, O. (1995) Horseradish peroxidase extraction and purification by aqueous two-phase partition. *Appl. Biochem. Biotechnol.* 53, 147–154.
- (31) Patel, M., Liang, L. P., and Roberts, L. J. (2001) Enhanced hippocampal F2-isoprostanate formation following kainite induced seizures. *J. Neurochem.* 79, 1065–1069.
- (32) SAS (1982) *SAS User's Guide: Statistics Edition*, SAS Institute Inc., Cary, NC.
- (33) Creighton, J. A., and Eadon, D. G. (1991) Ultraviolet-visible absorption spectra of the colloidal metallic elements. *J. Chem. Soc., Faraday Trans.* 87, 3881–3891.
- (34) Lyon, J. L., Fleming, D. A., Stone, M. B., Schiffer, P., and Williams, M. E. (2004) Synthesis of Fe oxide core/Au shell nanoparticles by iterative hydroxylamine seeding. *Nano Lett.* 4, 719–723.
- (35) Cheng, G., and Hight Walker, A. R. (2007) Synthesis and characterization of cobalt/gold bimetallic nanoparticles. *J. Mag. Mag. Mater.* 311, 31–35.
- (36) Bao, Y., Calderon, H., and Krishnan, K. M. (2007) Synthesis and characterization of magnetic-optical Co-Au core-shell nanoparticles. *J. Phys. Chem. C* 111, 1941–1944.
- (37) Zhou, W., Kumbhar, A., Wiemann, J., Fang, J., Carpenter, E. E., and O'Conner, C. J. (2001) Gold-coated iron (Fe@Au) nanoparticles: synthesis, characterization, and magnetic field-induced self-assembly. *J. Solid State Chem.* 159, 26–31.
- (38) Templeton, A. C., Pietron, J. J., Murray, R. W., and Mulvaney, P. (2000) Solvent refractive index and core charge influences on the surface plasmon absorbance of alkanethiolate monolayer-protected gold clusters. *J. Phys. Chem. B* 104, 564–570.
- (39) Averitt, R. D., Westcott, S. L., and Halas, N. J. (1999) Linear optical properties of gold nanoshells. *J. Opt. Soc. Am. B* 16, 1824–1832.
- (40) Vollmer, M. (1997) *Optical Spectroscopy of Metal Clusters*, Springer, Berlin.
- (41) Boyer, P., Ménard, D., and Meunier, M. (2010) Nanoclustered Co-Au particles fabricated by femtosecond laser fragmentation in liquids. *J. Phys. Chem. C* 114, 13497–1350.
- (42) Balasubramanian, S. K., Jittiwat, J., Manikandan, J., Ong, C. N., Yu, L. E., and Ong, W. Y. (2010) Biodistribution of gold nanoparticles and gene expression changes in the liver and spleen after intravenous administration in rats. *Biomaterials* 31, 2034–2042.
- (43) Cho, W. S., Kim, S., Han, B. S., Son, W. C., and Jeong, J. (2009) Comparison of gene expression profiles in mice liver following intravenous injection of 4 and 100 nm-sized PEG-coated gold nanoparticles. *Toxicol. Lett.* 191, 96–102.
- (44) De Jong, W. H., Hagens, W. I., Krystek, P., Burger, M. C., Sips, A. J., and Geertsma, R. E. (2008) Particle size-dependent organ distribution of gold nanoparticles after intravenous administration. *Biomaterials* 29, 1912–1919.
- (45) Garnett, M. C., and Kallinteri, P. (2006) Nanomedicines and nanotoxicology: some physiological principles. *Occup. Med.* 56, 307–311.
- (46) Cho, W. S., Cho, M., Jeong, J., Choi, M., Cho, H. Y., Han, B. S., Kim, S. H., Kim, H. O., Lim, Y. T., Chung, B. H., and Jeong, J. (2009) Acute toxicity and pharmacokinetics of 13 nm-sized PEG-coated gold nanoparticles. *Toxicol. Appl. Pharmacol.* 236, 16–24.
- (47) Khalil, W. K. B., Girgis, E., Emam, A. N., Mohamed, M. B., and Rao, K. V. (2011) Genotoxicity evaluation of nanomaterials: DNA

damage, micronuclei, and 8-hydroxy-2-deoxyguanosine induced by magnetic doped CdSe quantum dots in male mice. *Chem. Res. Toxicol.* 24, 640–650.

(48) Zhu, X., Zhou, W., Cui, Y., Zhu, L., Li, J., Feng, X., Shao, B., Qi, H., Zheng, J., Wang, H., and Chen, H. (2010) Pilocarpine protects cobalt chloride-induced apoptosis of RGC-5 cells: involvement of muscarinic receptors and HIF-1 alpha pathway. *Cell. Mol. Neurobiol.* 30, 427–435.

(49) Singh, N., Manshian, B., Jenkins, G. J. S., Griffiths, S. M., Williams, P. M., Maffeis, T. G. G., Wright, C. J., and Doak, S. H. (2009) NanoGenotoxicology: The DNA damaging potential of engineered nanomaterials. *Biomaterials* 30, 3891–3914.

(50) Valko, M., Rhodes, C. J., Moncol, J., Izakovic, M., and Mazur, M. (2006) Free radicals, metals and antioxidants in oxidative stress-induced cancer. *Chem.-Biol. Interact.* 160, 1–40.

(51) Zastawny, T. H., Altman, S. A., Randers-Eichhorn, L., Madurawe, R., Lumpkin, J. A., and Dizdaroglu, M. (1995) et al. DNA base modifications and membrane damage in cultured mammalian cells treated with iron ions. *Free Radical Biol. Med.* 18, 1013–1022.

(52) Kang, S. J., Kim, B. M., Lee, Y. J., and Chung, H. W. (2008) Titanium dioxide nanoparticles trigger p53-mediated damage response in peripheral blood lymphocytes. *Environ. Mol. Mutagen.* 49, 399–405.

(53) Schaeublin, N. M., Braydich-Stolle, L. K., Schrand, A. M., Miller, J. M., Hutchison, J., Schlager, J. J., and Hussain, S. M. (2011) Surface charge of gold nanoparticles mediates mechanism of toxicity. *Nanoscale* 3, 410–420.

(54) Johnston, H. J., Hutchison, G., Christensen, F. M., Peters, S., Hankin, S., and Stone, V. (2010) A review of the in vivo and in vitro toxicity of silver and gold particulates: Particle attributes and biological mechanisms responsible for the observed toxicity. *Crit. Rev. Toxicol.* 40, 328–346.

(55) Liu, Y., Meyer-Zaika, W., Franzka, S., Schmid, G., Tsoli, M., and Kuhn, H. (2003) Gold cluster degradation by the transition of B-DNA into A-DNA and the formation of nanowires. *Angew. Chem., Int. Ed.* 42, 2853–2857.

(56) Tsoli, M., Kuhn, H., Brandau, W., Esche, H., and Schmid, G. (2005) Cellular uptake and toxicity of Au55 clusters. *Small* 1, 841–844.

(57) Goodman, C. M., Chari, N. S., Han, G., Hong, R., Ghosh, P., and Rotello, V. M. (2006) DNA binding by functionalized gold nanoparticles: mechanism and structural requirements. *Chem. Biol. Drug Des.* 67, 297–304.

(58) Newmann, M. C., and Clements, W. H. (2008) Stress-Based Theories of Aging, in *Ecotoxicology: A Comprehensive Treatment*, p 290, CRC Press, Taylor and Francis Group, New York.

(59) Young, I. S., and Woodside, J. V. (2001) Antioxidants in health and disease. *J. Clin. Pathol.* 54, 176–186.